Third International Symposium on Marine Propulsors
smp'13, Launceston, Tasmania, Australia, May 2013

Numerical investigation of ducted propeller added mass.

Suzanne Hutchison[1], Sverre Steen[1] and Abhishek Sanghani[2]

[1]Department of Marine Technology, Norwegian University of Science and Technology (NTNU), Trondheim, Norway
[2]Department of Ocean Engineering and Naval Architecture, Indian Institute of Technology (IIT) Kharagpur, India

ABSTRACT

This paper investigates the effect of a duct on propeller added mass by comparing the propeller and duct individually with the bodies combined in a multi-body simulation. This is a preliminary step towards better understanding of the loads and responses of a ducted azimuthing thruster in various extreme load cases and developing a multi-body simulation model of the thruster with internal drive train. The numerical analysis is conducted with the commercial DNV software HydroD, using its WADAM program. The results show that the propeller is more affected by the presence of the duct than the duct is affected by the presence of the propeller. The presence of the duct on the propeller increases the uncoupled added mass linear terms by 10% and rotational terms by 33% when compared with the propeller added mass in isolation. The influence of propeller on the duct is relatively minor with the added mass changing less than 3.5% for all uncoupled terms when compared with the duct added mass in isolation. Once the bodies are considered to move independently of each other the effect of each body on the other is greatly increased with a change in the coupled added mass terms up to 133%.

Keywords

Propeller, duct, added mass, and multibody simulation.

1 INTRODUCTION

In order to better estimate the loads and responses of a ducted azimuthing thruster in various extreme load cases, a Multi-Body Simulation (MBS) model of the thruster with internal drive train is being developed. An important part of such a MBS model is a fast and accurate model of the hydrodynamic loads on the propeller and duct. The hydrodynamic added mass and damping of the propeller and duct are important parts of the hydrodynamic load model. To develop such a fast numerical hydrodynamic model for MBS the accuracy and complexity of hydrodynamic added mass needs to be determined. The accuracy of the hydrodynamic model needs to be sufficient to capture the physics but calculated in a short time frame to make the MBS feasible. MBS involves the modelling of the complete propulsion system from the motor to the propeller including the mechanical coupling of gear rotors, shafts and other structural components. MBS is used to understand the complexities of the system as a whole for instance the effect of added mass and damping of the propeller on the natural frequencies and dynamic responses of the propulsion system. Specifically, how are the loads from the propeller transmitted and is the response extreme enough to cause a translation or change in rotation in all or part of the propulsion system drive train?

To determine the contribution of radiation forces and the natural frequencies of oscillation in various degrees of freedom, accurate data on added mass matrices of a body is important for its vibrational analysis. Such an analysis is frequently done at the various design stages of floating or submerged bodies.

No previous study of the added mass of a propeller and a duct as a whole has been found. Most of the work available in the literature, discussing added mass of propellers reports them considering no rotation. There are several well-known publications discussing the added mass and damping of open propellers. Some of the most well-known experiments on propeller added mass were conducted by Burrill & Robson (1962) on the KCA series in the locked (non-rotating) condition. This work investigated the axial and torsional added mass but did not account for the coupling between the added mass directions. Theoretical and analytical solutions for the added mass of an open propeller include Schwanecke (1963) and Parsons & Vorus (1981). In some cases the differences between the theoretical solution and comparison with experiment can be as large as 20%, Ghassemi & Yari (2011). The evaluation of added mass matrices for a single body and multi body systems is discussed by Korotkin (2009) in his book. Various cases of planar contours, three dimensional bodies, interacting bodies and propeller are considered.

A review of the calculation methods that are available to estimate the added mass properties of a propeller for vibrational analysis is provided by MacPherson et al. (2007). It critically examines values available from various experimental and theoretical analyses and also considers the effect of rotation.

Kerwin et al. (1987) discussed methods for hydrodynamic analysis of ducted propellers. These can be largely adapted

for the development of a program which includes the forward velocity and evaluates the added mass matrices of a ducted propeller system, using surface panel methods. The wave effects on a system of bodies located in close proximities with hydrodynamic interactions and solutions based on panel methods and other direct numerical methods are reviewed by Newman (2001). This work gives a fair idea of the evolution of our understanding of multi body systems.

The motivation to study a non-rotating ducted propeller, with zero forward speed, comes from the description of the effect of angular velocity and forward speed on the added mass values of an open propeller as reported by Zhiqiang & Rixiu (1996). For an open propeller, it was shown that the effect of vibration frequencies was pronounced in the low frequency region, and became very small as the vibration frequency approached infinity. It was also shown that for a given advance coefficient, the added mass coefficients remained unchanged with different combinations of rotation velocity and advance speed.

This paper is presented in seven sections; first the theory and the assumptions of the software are introduced and then the software implementation is discussed. The discussion of the validation and results follows. The results section of the paper is presented for the propeller and duct individually and then for the combined geometry. This paper is concluded by a section of the overall conclusions from the study.

2 Theory and Assumptions

The fluid is assumed to be inviscid, incompressible, and flow is irrotational. The propeller and duct are assumed to be rigid bodies. The propeller is considered locked (non-rotating) with zero forward speed and therefore in the sub-cavitation range. The hydrodynamic interactions are computed using the linear potential theory.

In potential theory, the fluid velocity is defined as the gradient of the velocity potential. Assuming a perturbation solution in terms of small wave slope of incident waves, the velocity potential is expanded in a form Lee (2005):

$$\Phi\left(x,t\right)=\Phi^{(1)}(x,t)+\Phi^{(2)}\left(x,t\right)+\cdots \tag{1}$$

Where $\Phi\left(x,t\right)$ = velocity potential; t = time; and $x = (x,y,z)$ = denotes the Cartesian coordinates of a point in space.

The motion amplitude (about the mean position), consisting of the six modes of rigid body motion. The free surface elevation (about the mean free surface) is also expanded similarly.

In a linearized potential theory, only the first order term of equation 1 is considered. The total first order potential for wave-body interaction can be expressed as a sum of components with different circular frequencies $\omega_j > 0$.

$$\Phi^{(1)}\left(x,t\right)=Re\sum\Phi_j(x)e^{(i\omega_j t)} \tag{2}$$

Where, Φ_j is the complex velocity potential, independent of time, with the real part of the time harmonic solution being physically relevant. The Φ_j denotes the first order solution in the presence of the incident wave of frequency ω_j and wave heading β_j.

Due to linearity, Φ_j can be expressed as a sum of the diffraction velocity potential (Φ_D) and the radiation velocity potential (Φ_R). The diffraction velocity potential (Φ_D) is defined as the sum of the incident velocity potential (Φ_I) of the first order incident wave, and the scattering velocity potential (Φ_S). Numerically,

$$\Phi=\Phi_I+\Phi_S+\Phi_R=\Phi_D+\Phi_R \tag{3}$$

For the simple case of a single body with six degrees of freedom, the radiation potential is written as a summation of contributions from individual modes as:

$$\Phi_R=i\omega\sum_{k=1}^{6}\xi_k\Phi_k \tag{4}$$

where ξ_k is the complex amplitude of the oscillatory motion in the kth mode of the six degrees of freedom, and Φ_k is the corresponding unit amplitude linear or angular velocity of the rigid body motion. The kinematic boundary condition (i.e. no flow penetration) on the surface S is expressed as:

$$\frac{\partial\Phi_k}{\partial n}=n_k \tag{5}$$

And

$$\frac{\partial\Phi_S}{\partial n}=\frac{\partial\Phi_I}{\partial n} \tag{6}$$

Where, the unit vector $n=(n_1,n_2,n_3)$ is normal to the body boundary, pointing outwards on the fluid domain. The elements n_4,n_5,n_6 for $k>3$ are defined as $(n_4,n_5,n_6)=x\times n$. From equation 3, it follows that:

$$\frac{\partial\Phi_D}{\partial n}=0 \tag{7}$$

The hydrodynamic pressure force (and moment) acting on the body are represented by the exciting force (due to $\Phi_D^{(1)}$):

$$X_i=-i\omega\rho\left(\iint\Phi_D n_i dS\right)_S \tag{8}$$

And by the added mass and damping (due to$\Phi_R^{(1)}$):

$$A_{ij}-\left(i/\omega\right)B_{ij}=\rho\left(\iint\Phi_j n_i dS\right)_S \tag{9}$$

The radiation-diffraction part of Wadam is based on WAMIT. From Lee (2005) the convention used for multi body analysis, is to extend the notation by defining Φ_k as the velocity potential corresponding to a particular mode of one body, while the other bodies are kept stationary. Therefore, the total radiation potential consists of $6N$ components, N being the number of bodies, which is two in our case.

The boundary value problem is solved using the method of integral equations for the source strength σ_k and σ_s corresponding to the radiation potential Φ_k and scattering potential Φ_s respectively. The integral equation for σ_k is:

$$2\pi\sigma_k(x) + \left(\iint d\xi \sigma_k(\xi) \left(\partial G(\xi; x)/\partial n_x \right) \right)_{S_B} = n_k \tag{10}$$

And for σ_s is:

$$2\pi\sigma_s(x) + \left(\iint d\xi \sigma_k(\xi) \left(\partial G(\xi; x)/\partial n_x \right) \right)_{S_B} = \frac{\partial \Phi_I}{\partial n} \tag{11}$$

The fluid velocity on the body boundary or in the fluid domain due to Φ_k or Φ_S is then obtained from:

$$\nabla\Phi(x) = \nabla \left(\iint d\xi \sigma_k(\xi) \left(\partial G(\xi; x)/\partial n_x \right) \right)_{S_B} \tag{12}$$

Here $G(\xi, x)$; is the Green function, which is referred to as the wave source potential or the velocity potential at the point x due to a source of strength -4π located at the point ξ.

The integral equations are solved by the panel method. The wetted body surface is represented by an ensemble of quadrilateral panels (a triangular panel is a special type of quadrilateral panel where two vertices coalesce), and the integral equation is enforced at the centroid of each panel (a collocation method).

3 Software implementation

The main aim of this paper is to isolate the effect of the presence of a duct on the locked propeller added mass. This is achieved by comparing the added mass matrix of the individual bodies of the propeller and duct model to a multi body model. The numerical simulation was undertaken in the commercial DNV software HydroD V4.5-08, using its WADAM program. The present approach with many simplifying assumptions is chosen as a preliminary step to understand the problem of calculating added mass matrices of the duct and propeller multi-body system.

Validation of the propeller model is undertaken by comparing the numerical results with experimental results by Burrill & Robson (1962) and previous theoretical and analytical results by Schwanecke (1963) and Parsons & Vorus (1981). To ensure that the analysis addressed the issue of small gap between the tip of the propeller and the duct boundary, validation was conducted by comparing the numerical results to the results by Yamamoto et al. (1974) showing the variation of the added mass of a cylinder in close proximity of the sea floor.

3.1 Co-ordinate System

The global coordinate system in WADAM is a right handed Cartesian coordinate system with its origin at the still water level and with the z-axis normal to the still water level and the positive z-axis pointing upwards. For this analysis, the propeller and duct were translated such that their centreline was 10 m below the free surface. Thus their centre of gravity lied 10 m below the free surface. The water depth was kept at 300 m. Although within WADAM the result reference point can be chosen by the user in single body analysis, the multi-body analysis results are reported in the global coordinate system only. A transformation is then used to report the added mass values in a body fixed coordinate system centred at the centre of gravity. For this analysis is taken same as the centre of buoyancy of the propeller at (8.19E-02, 3.46E-04, -1.00E+01) with respect to the global origin. The body fixed co-ordinates for the propeller is shown in Figure 1.

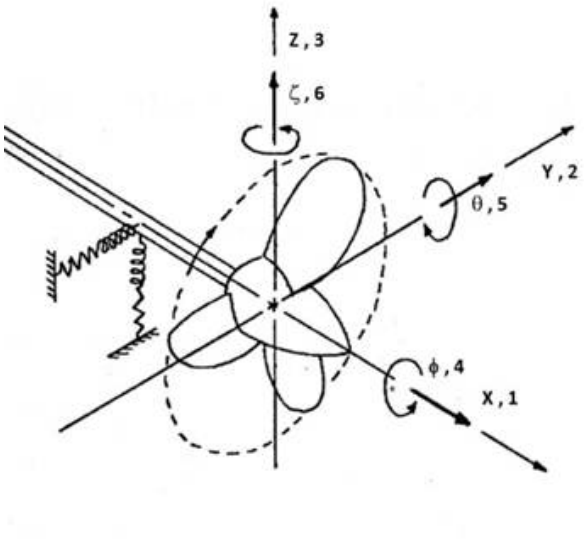

Figure 1: Propeller co-ordinates Parsons & Vorus (1981)

4 Input data

4.1 Propeller

Numerical analysis was carried out on a four-bladed propeller with a generic geometry, P-1374 designed by MARINTEK. For more details see Amini (2011). This propeller is designed to operate with or without a duct. The original design was scaled up to a full scale propeller with a diameter (D_P) of 4 m. The hub diameter was 960 mm, therefore r_h/R is 0.24 (r_h is the hub radius). The design pitch ratio (P/D_P) was 1.1 and expanded blade area ratio (A_E/A_O) was 0.6. The propeller had a skew of 25 degrees.

4.2 Duct

The duct used was a typical 19A design. It is a general purpose duct for application at heavy screw loads. The nozzle has a cylindrical inner side, the outside is straight and the trailing edge is relatively thick. The length ratio is 0.5. The duct was designed to full scale with the inner diameter (D_D) to be 4.04 m, such that the tip gap between the propeller and duct was 20 mm.

5 Problem definition

5.1 Mesh

The mesh was generated using the DNV software Genie V5.3-10. The propeller mesh with a size of 2489 elements is shown in Figure 2.

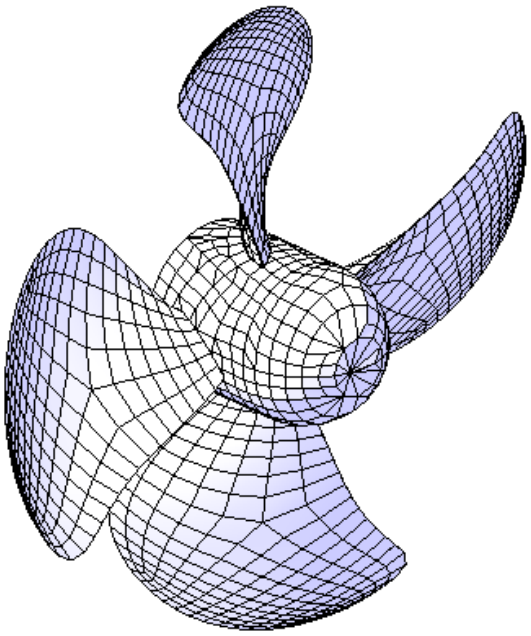

Figure 2: Panel mesh of the propeller

The mesh for the duct with a size of 11501 elements is shown in Figure 3. The duct mesh was constrained to have a finer mesh on the inner side, where the gap between the propeller and the duct was least.

Figure 3: Panel mesh of the duct

The model of both the propeller and the duct used the same mesh that was generated for the individual models, the resulting model is shown in Figure 4.

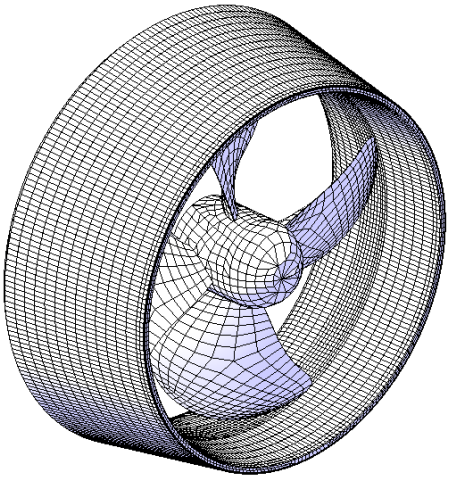

Figure 4: Panel mesh of the propeller and duct combined

6 Discussion and Results

6.1 Validation

Comparisons with previous propeller data is discussed in the next section. In this section the validation of two bodies in close proximity is undertaken by modelling a cylinder close to the wall with 2D analytical results available from the literature by (Yamamoto et al., 1974). For a long cylinder, let the 2D added mass in sway and heave be denoted by $A^C = A^C_{22} = A^C_{33}$. And let the coefficient of added mass in sway and heave be denoted by $a^C = a^C_{22} = a^C_{33}$. Therefore, the relation between the two is:

$$A^C = \rho a^C(\pi r^2) \tag{13}$$

Where, r is the radius of the cross section, and πr^2 is area of the cross section of the cylinder. Theoretically, for a long cylinder, $a^C = 1$. As the cylinder is brought closer to a wall, its value should increase and reach 2.29, for no gap between the wall and the cylinder. Due to a limit in the number of panels that could be analyzed in a single analysis, instead of a long cylinder, we used a cylinder of length of 20 m and diameter of 2 m, so that, $r/L = 0.05$. As such, we expected the value of a^C to be slightly less than 1. Also, we expected that the added masses in heave (a^C_{33}) and sway (a^C_{22}) to be unequal as the cylinder reached the bottom. We also expected their magnitudes to rise and show a similar trend, as is seen for a long cylinder. The ratios $a^C_{22}/a^{C\infty}_{22}$ and $a^C_{33}/a^{C\infty}_{33}$, as obtained from the analysis, are shown as a function of the distance of the cylinder from the ground in Table 1. The distance between the cylinder surface and ground (e), is presented in the form of the ratio e/D, where D is the diameter of the cylinder.

Table 1: Added mass of a cylinder in close proximity to a wall

e/D	Sway HydroD	Heave HydroD	Approx. (Yamamoto et al., 1974)	%diff Sway	%diff Heave
75	1.000	1.000	1	0 %	0 %
1	1.043	1.056	1.078	-3 %	-2 %
0.5	1.111	1.135	1.135	-2 %	0 %
0.25	1.223	1.262	1.2475	-2 %	1 %
0.00781	1.875	2.015	2.1798	-14 %	-8 %
0.00391	1.950	2.102	2.180	-11 %	-4 %
0	2.153	2.310	2.229	-3%	4 %

A comparison of HydroD and results from Yamamoto et al. (1974) is shown in Figure 5.

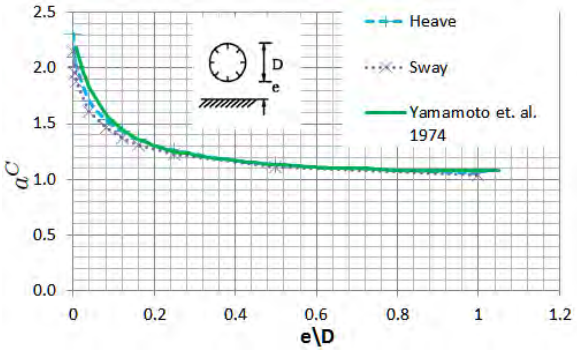

Figure 5: Comparison of added mass of a circular cylinder near a wall as computed with HydroD and as published by Yamamoto et al. (1974)

As expected this shows HydroD predicts a lower added mass co-efficient as the cylinder approached the wall. At an e/D ratio of 0.04 the HydroD added mass prediction is 11% lower in heave and 17% lower in sway than the 2D results. Analysis of the added mass of a cylinder with slenderness ratio of $r/L = 0.05$ and comparison with analytical 2-D results verifies that we are able to predict added mass using HydroD with high accuracy, and that our procedure is capable of capturing changes in the added mass values in systems with small tip gaps.

6.2 Results

In this section a superscript 'P' is used to indicate the propeller, and similarly 'D' to indicate the duct.

6.2.1 Propeller

The added mass coefficients (a_{ij}) of the 'locked' propeller is reported in this section, and compared to results by Burrill & Robson (1962), Schwanecke (1963) and Parsons & Vorus (1981). These results have been non-dimensionalized by dividing the added mass values (A_{ij}) by the factors given in in Table 2.

Table 2: Factors to non-dimensionalising the added mass values (A_{ij}) Parsons & Vorus (1981)

Factor	Corresponding i and j number in A_{ij}	Type of coefficient
ρD^3	i = 1,2,3 ; j = 1,2,3	added mass
ρD^4	i = 1,2,3 ; j = 4,5,6 or j = 1,2,3 ; i = 4,5,6	inertia coupling
ρD^5	i = 4,5,6 ; j = 4,5,6	added mass moment of inertia

The general form of the added mass matrix for a propeller is shown in Table 3.

Table 3: General form of the added mass matrix for a propeller (Carlton, 2007)

	1	2	3	4	5	6
1	a^P_{11}	0	0	a^P_{41}	0	0
2	0	a^P_{22}	$-a^P_{32}$	0	a^P_{52}	$-a^P_{62}$
3	0	a^P_{32}	a^P_{22}	0	a^P_{62}	a^P_{52}
4	a^P_{41}	0	0	a^P_{44}	0	0
5	0	a^P_{52}	$-a^P_{62}$	0	a^P_{55}	$-a^P_{65}$
6	0	a^P_{62}	a^P_{52}	0	a^P_{65}	a^P_{55}

The propeller was modelled as a single body in WADAM and the added mas results are presented in Table 4.

Table 4: Results (a^P) from numerical analysis in WADAM

	1	2	3	4	5	6
1	0.0717	0	0	-0.0108	0.0007	0
2	0	0.0223	0.0001	-0.0002	0.0055	-0.0003*
3	0	-0.0003	0.0225	0	0.0003*	0.0055
4	-0.0108	-0.0002	0	0.0019	-0.0005	0
5	0.0007	0.0056	0.0004*	0.0002	0.0033	0
6	0	-0.0004*	0.0056	-0.0001	0	0.0033

If we consider the results in Table 4 and the propeller is symmetrical we notice values (in grey without a superscript) are not equal in the pairs of symmetry ($a^P_{32} \neq -a^P_{23}$, $a^P_{42} \neq a^P_{43}$, $a^P_{45} \neq a^P_{46}$ and $a^P_{51} \neq a^P_{61}$) and these values should be disregarded. If we consider that this lack of symmetry is due to numerical error then results from WADAM are accurate to the thousandths figure. Therefore all remaining results from WADAM are presented to this accuracy and results a^P_{62} and a^P_{52} indicated in grey with a '*' superscript in Table 4 become 0. The modified results are shown in Table 5.

Table 5: Results (a^P) from numerical analysis in WADAM to the thousandths figure

	1	2	3	4	5	6
1	0.072	0	0	-0.011	0	0
2	0	0.022	0	0	0.006	0
3	0	0	0.022	0	0	0.006
4	-0.011	0	0	0.002	0	0
5	0	0.006	0	0	0.003	0
6	0	0	0.006	0	0	0.003

Results calculated using the equations obtained from the regression by Parsons & Vorus (1981) (a_P^P), without the lifting surface corrections is shown in Table 6.

Table 6: Results (a_P^P) calculated using the equations obtained from the regression by Parsons & Vorus (1981)

	1	2	3	4	5	6
1	0.069	0	0	-0.012	0	0
2	0	0.0162	-0.0007	0	0.0058	-0.0002
3	0	0.0007	0.0162	0	0.0002	0.0058
4	-0.012	0	0	0.002	0	0
5	0	0.0058	-0.0002	0	0.0033	-0.0002
6	0	0.0002	0.0058	0	0.0002	0.0033

To compare Parsons & Vorus (1981) to our simulation results the percentage difference is presented in Table 7. The largest percentage difference is for sway and heave (a_{22}^P).

Table 7: Percentage difference between a^P in Table 5 and a_P^P in Table 6

	1	2	3	4	5	6
1	4.17	-	-	-9.09	-	-
2	-	27.27	-	-	0.00	-
3	-	-	27.27	-	-	0.00
4	-9.09	-	-	0.00	-	-
5	-	0.00	-	-	0.00	-
6	-	-	0.00	-	-	0.00

The values are also compared with the theoretical predictions from Schwanecke (1963), which considers unsteady propeller theories. In his formulation, he did not take into account the coupling between lateral motions. The added mass matrix as predicted from the Schwanecke (1963) is shown in Table 8

Table 8: Results (a_s^P) as predicted from the Schwanecke (1963) formulation

	1	2	3	4	5	6
1	0.0795	0	0	-0.0139	0	0
2	0	0.0221	0	0	0.007	-0.0022
3	0	0	0.0221	0	0.0022	0.007
4	-0.0139	0	0	0.0024	0	0
5	0	0.007	-0.0022	0	0.0035	-0.0001
6	0	0.0022	0.007	0	0.0001	0.0035

To compare Schwanecke (1963) to our simulation results the percentage difference is presented in Table 9. The largest percentage difference is for the inertia coupling terms.

Table 9: Percentage difference between a^P in Table 5 and a_s^P in Table 8

	1	2	3	4	5	6
1	-11.11	-	-	-27.27	-	-
2	-	0.00	-	-	-16.67	-
3	-	-	0.00	-	-	-16.67
4	-27.27	-	-	0.00	-	-
5	-	-16.67	-	-	-33.33	-
6	-	-	-16.67	-	-	-33.33

The data from the Burrill & Robson (1962) tests was used to give empirical relationships between the axial and torsional added mass values and propeller parameters. MacPherson et al. (2007) using these estimates published a more accurate formulation for added mass coefficients based on an empirical relationship in the following form:

$$a_{11}^P = \frac{C_1 \left(\frac{A_E}{A_O}\right)}{5 + \left(\frac{P}{D_P}\right)^2} - C_2 \tag{14}$$

Table 10: MacPherson et al. (2007) coefficients for Burrill & Robson (1962) estimate of added mass in axial vibration

	Z = 3	Z = 4	Z = 5	Z = 6
C_1	1.0638	0.9553	0.9104	0.8588
C_2	0.023	0.03	0.032	0.033

$$a_{44}^P = C_1 \left(\frac{A_E}{A_O}\right)\left(\frac{P}{D_P}\right) - C_2 \tag{15}$$

Table 11: MacPherson et al. (2007) coefficients for Burrill & Robson (1962) estimate of added mass in torsional vibration

	Z = 3	Z = 4	Z = 5	Z = 6
C_1	0.00477	0.00394	0.00359	0.00344
C_2	0.00093	0.00087	0.0008	0.00076

An additional comparison of the numerical method was undertaken using MacPherson et al. (2007) from equations 14 and 15. Using these, the added mass values for our test propeller are:

$$a_{11}^P = 0.062 \qquad a_{44}^P = 0.002 \qquad (16)$$

As a percentage difference from the original results this is a difference of $a_{11}\%_{diff} = 14\%$ and $a_{44}\%_{diff} = 0\%$. The Burrill & Robson (1962) experiments involved thinner rods with a r_h/R_P 0.0234. This is much smaller than our value of 0.24. The validation of our results against published data for open propeller shows that we get results that have reasonably good agreement. There are differences in geometry and also uncertainties related to the accuracy of the data we compare with. We conclude, that the above analysis accurately describes the added mass matrices for a propeller, based on linearized potential theory for the system with non-rotating propeller.

6.2.2 Duct

The added mass coefficients (a_{ij}^D) of the duct is presented in Table 12. Results are non-dimensional and presented to the thousandth figure using the same process as for the propeller.

Table 12: Added mass coefficients (a_{ij}^D) of the duct from numerical analysis

	1	2	3	4	5	6
1	0.029	0	0	0	0	0
2	0	0.289	0	0	0	-0.015
3	0	0	0.289	0	0.015	0
4	0	0	0	0	0	0
5	0	0	0.015	0	0.008	0
6	0	-0.015	0	0	0	0.008

As one can note, the added mass in surge is almost 10 times less than the added masses in sway and heave, which are the same value. Similarly, the added moment of inertia in roll is zero due to the duct being a body of rotation. The added moment of inertia in pitch and yaw are identical due to symmetry.

6.2.3 Propeller and Duct

The added mass matrix for the propeller and duct as parts of the multi-body system takes the form of a 12 x 12 matrix. To present the data this matrix has been divided into 4 parts. The notation for these matrices is a^{12} where the '1' indicates the body that the added mass is given for and the '2' indicates the body that is oscillated. This results in the following four dimensionless matrices:

a^{PP} : Matrix of added mass coefficients for the propeller, due to unit oscillation of propeller about its mean position.

a^{PD} : Matrix of added mass coefficients for the propeller, due to unit oscillation of duct about its mean position.

a^{DP} : Matrix of added mass coefficients for the duct, due to unit oscillation of propeller about its mean position.

a^{DD} : Matrix of added mass coefficients for the duct, due to unit oscillation of duct about its mean position.

Therefore a^{PP} and a^{PD} in Tables 13 and 14 are reported with respect to the origin at propeller, and are non-dimensional results of the corresponding A^{PP} and A^{DP} with the factors given in Table 3. Similarly for a^{DD} and a^{DP} in Tables 15 and 16.

Table 13: a^{PP}: Matrix of added mass coefficients of propeller, due to unit oscillation of propeller about its mean position

	1	2	3	4	5	6
1	0.079	0	0	-0.012	0	0
2	0	0.024	0	0	0.006	0
3	0	0	0.024	0	0	0.006
4	-0.012	0	0	0.002	0	0
5	0	0.006	0	0	0.004	0
6	0	0	0.006	0	0	0.004

Table 14: a^{PD}: Matrix of added mass coefficients of propeller, due to unit oscillation of duct about its mean position

	1	2	3	4	5	6
1	0.009	0	0	0	0	0
2	0	-0.013	0.001	0	-0.002	0.001
3	0	-0.001	-0.013	0	-0.001	-0.002
4	0	0.001	0	0	-0.013	0
5	0	0.006	-0.003	0.035	0.004	0
6	0	0.003	0.006	0	0	0.004

Table 15: a^{DD}: Matrix of added mass coefficients of duct, due to unit oscillation of duct about its mean position

	1	2	3	4	5	6
1	0.030	0	0	0	0	0
2	0	0.291	0	0	-0.001	-0.015
3	0	0	0.291	0	0.015	-0.001
4	0	0	0	0	0	0
5	0	-0.002	0.059	0	0.008	0
6	0	-0.059	-0.002	0.001	0	0.008

Table 16: a^{DP}: Matrix of added mass coefficients of duct, due to unit oscillation of propeller about its mean position

	1	2	3	4	5	6
1	0.009	0	0	0	0	0
2	0	-0.013	-0.001	0	0.001	0
3	0	0.002	-0.013	0	0	0.001
4	-0.001	0	0	0	0.003	0
5	0	-0.002	-0.001	-0.009	0.001	0
6	0	0.001	-0.002	0.001	0	0.001

In Tables 14, 15 and 16 we notice that the matricies have become non-symmetric for example in Table 16 $a^{DP}_{52} \neq a^{DP}_{25}$, $a^{DP}_{62} \neq a^{DP}_{26}$, $a^{DP}_{53} \neq a^{DP}_{35}$ and $a^{DP}_{63} \neq a^{DP}_{36}$ this result was not expected. This asymmetry is particularly noticeable in a^{DD} as shown in Table 15. These results have not been included in any of the following comparisons.
To get a clearer idea of the difference in values, the percentage change in the added mass values are given in Tables 17, 18, 20, and 19 as per the following equations:

$$a^{PP}_{rel} = (a^P - a^{PP})/a^P \times 100 \quad (17)$$

$$a^{PD}_{rel} = (a^{PD})/a^P \times 100 \quad (18)$$

$$a^{DD}_{rel} = (a^D - a^{DD})/a^D \times 100 \quad (19)$$

$$a^{DP}_{rel} = (a^{DP})/a^D \times 100 \quad (20)$$

Table 17: a^{PP}_{rel}: Percentage difference between a^{PP} and a^P with respect to a^P

	1	2	3	4	5	6
1	-9.72	-	-	-9.09	-	-
2	-	-9.09	-	-	0.00	-
3	-	-	-9.09	-	-	0.00
4	-9.09	-	-	0.00	-	-
5	-	0.00	-	-	-33.33	-
6	-	-	0.00	-	-	-33.33

From the presented analysis, it is found that the values of the added mass matrix of the propeller (a^{PP}) increase due to the presence of the duct. The values of the linear added mass terms and a^P_{41} of the matrix increasing by approximately 9% and the added mass moment of inertia about axes 5 and 6 increase by 33%.

Table 18: a^{PD}_{rel}: Percentage difference between a^{PD} and a^P with respect to a^P

	1	2	3	4	5	6
1	12.50	-	-	0.00	-	-
2	-	-59.09	-	-	-	-
3	-	-	-59.09	-	-	-
4	0.00	-	-	0.00	-	-
5	-	-	-	-	133.33	-
6	-	-	-	-	-	133.33

The added mass matrix for a^{PD} shows an increase in the diagonal axes and similarly to (a^{PP}). The added mass moment of inertia about axes 5 and 6 showed the largest influence with an increase of 133%. The differencs in the added mass matrix for a sway and heave (a^{PD}_{22}) is influenced more than that in surge (a^{PD}_{11}).

Table 19: a^{DD}_{rel}: Percentage difference between a^{DD} and a^D with respect to a^D

	1	2	3	4	5	6
1	-3.45	-	-	-	-	-
2	-	-0.69	-	-	-	-
3	-	-	-0.69	-	-	-
4	-	-	-	-	-	-
5	-	-	-	-	0.00	-
6	-	-	-	-	-	0.00

The influence of the propeller on the duct is shown to be less than the influence of the duct on the propeller in Tables 17 and 19.

Table 20: a^{DP}_{rel}: Percentage difference between a^{DP} and a^D with respect to a^D

	1	2	3	4	5	6
1	31.03	-	-	-	-	-
2	-	-4.50	-	-	-	-
3	-	-	-4.50	-	-	-
4	-	-	-	-	-	-
5	-	-	-	-	12.50	-
6	-	-	-	-	-	12.50

The influence of the propeller on the duct is greatest when the propeller is moving as shown in Table 20, the greatest influence is in surge a^{DP}_{11}.

7 Conclusions

Analysis of the added mass of a cylinder with a slenderness ratio of 0.1 and comparison with analytical 2-D results ver-

ifies that we are able to predict the added mass using HydroD with high accuracy, and that our procedure is capable of capturing changes in the added mass values in systems with small tip gaps. From this analysis we can conclude that the presence of the duct does affect the added mass of the propeller. The effect of duct on the propeller is greater than the effect of the propeller on the duct. The presence of the duct on the propeller increases the uncoupled added mass linear terms by 10% and rotational terms by 33% when compared with the propeller added mass in isolation. The influence of propeller on the duct is relatively minor with the added mass changing less than 3.5% for all uncoupled terms when compared with the duct added mass in isolation. Once the bodies are considered to move independently of each other the effect of each body on the other is greatly increased with a change in the coupled added mass terms of up to 133%.

REFERENCES

Amini, H., 2011. Azimuth propulsors in off-design conditions. Ph.D. thesis, Norges teknisk-naturvitenskapelige universitet.

Burrill, L. & Robson, W., 1962. 'Virtual mass and moment of inertia of propellers'. Transactions North East Coast Institution of Engineers and Shipbuilders **78**.

Carlton, J., 2007. Marine propellers and propulsion. Butterworth-Heinemann, Oxford. 2nd ed.

Ghassemi, H. & Yari, E., 2011. 'The Added Mass Coefficient computation of sphere, ellipsoid and marine propellers using Boundary Element Method'. Polish Maritime Research **18**(1), pp. 17–26.

Kerwin, J. E., Kinnas, S. A., Lee, J.-T. & Shih, W.-Z., 1987. "A surface panel method for the hydrodynamic analysis of ducted propellers". Transactions of Society of Naval Architects and Marine Engineers, vol. 95.

Korotkin, A. I., 2009. Added Masses of Ship Structures. Springer Science and Business Media B.V.

Lee, C.-H., 2005. 'WAMIT THEORY MANUAL'. Tech. rep., Massachusetts Institute of Technology.

MacPherson, D., Puleo, V. & Packard, M., 2007. 'Estimation of entrained water added mass properties for vibration analysis'. SNAME New England Section .

Newman, J. N., 2001. 'Wave Effects on Multiple Bodies'. Kashiwagi, M. (ed.) Hydrodynamics in Ship and Ocean Engineering, vol. 3. pp. 3–26.

Parsons, M. G. & Vorus, W. S., 1981. 'Added Mass and Damping Estimates for Vibrating Propellers'. Propellers '81 Symposium. Transactions of Society of Naval Architects and Marine Engineers, p. 16.

Schwanecke, H., 1963. 'Gendanken zur frage der hydrodynamisch erreten schwingungen des propellers und der wellenleitung'. Yahrbuch der STG **57**.

Yamamoto, T., Nath, J. & Slotta, L., 1974. 'Wave forces on cylinders near plane boundary.' Journal Waterway, Port, Coastal Ocean Engineering Divisions, ASCE **100**.

Zhiqiang, S. & Rixiu, G., 1996. 'Hydroelasticity of Rotating Bodies - Theory and Application'. Marine Structures **9**(6), pp. 631–646.